Performance of p^+-n LWIR HgCdTe photodiodes

A. ROGALSKI, A. JÓŹWIKOWSKA, K. JÓŹWIKOWSKI and J. RUTKOWSKI

Institute of Technical Physics, WAT
01-489 Warszawa 49, Poland

1. Introduction

Hitherto, the realization of HgCdTe photodiodes has usually been based on an n^+-p structure. Theoretical reasons for the choice of the n^+-p configuration include the significantly longer minority carrier diffusion length in p-type material, and the possibility of achieving longer minority carrier lifetime in p-type material rather than in an n-type one of comparable carrier concentration. The most common technique for producing n^+-p junctions is to implant ions into p-type material.

In 1985, Rogalski and Larkowski [1, 2] indicated that due to the lower mobility of holes in the n-type region of p^+-n junctions with thick a n-type region, the diffusion limited R_oA product of such junctions is lager than of n^+-p junctions. Such theoretical predictions have been recently confirmed by experimental results obtained for p^+-n HgCdTe junctions [3, 7].

Wang's experimental results indicate that the performance of p-on-n and n-on-p photodiodes exhibit similar R_oA products at 77 K for $\lambda_c < 10$ μm. Instead of $\lambda_c < 10$ μm, the R_oA products of n-on-p photodiodes are generally inferior; their quantum efficiency is lower and the forward impedance is higher [7]. Wang suggests that these problems are probably caused by the relative immaturity in fabricating n-on-p heterojunctions, especially in the surface control on the p-side for diodes with a longer wavelength cutoff.

Recently, Pultz et al. [6] and Wang [7] have compared their experimental R_oA results with theory using a simple n-side diffusion model. In this paper a self-consistent iterative procedure has been used to analyze the performance of p^+-n-n^+ HgCdTe photodiodes: quantum efficiency and R_oA product. The considerations are carried out for the 40–77 K temperature region and 7–15 μm spectral region. Results of calculations are compared with experimental data reported by several authors.

2. Theory

Let us consider a typical high quality p^+-n-n^+ photodiode structure which can be fabricated using modern epitaxy growth techniques (LPE, MBE or MOCVD). In such a photodiode, the base n-type layer with resultant carrier concentration of about 10^{15} cm^{-3} and thickness of about 20 μm is sandwiched between high-doped regions. To receive high quantum efficiency, a 1-2-μm-thick p^+-type cap layers is usually grown with carrier concentration to 10^{18} cm^{-3}. By thinning the base n-type region of the photodiode to a thickness less than the diffusion length of the minority carriers (thus reducing the volume in which diffusion current is generated) the corresponding R_oA product increases, provided that the back junction is characterized by low recombination rate. The backside n-n^+ junction is "blocking" in nature; a more intensely doped region causes a built-in electric field that repels minority carriers, thereby reducing recombination.

For simplicity, we will take the one-dimensional model for the photodiode with ohmic electrical contacts. Figure 1 shows a doping profile of the photodiode described above. We assume that the uniform signal photon flux Φ_s is incident on the photodiode area A. The influence of assuming doping profile on photodiode performance has been solved by forward-condition steady-state analysis [8]. It was necessary to solve a certain d.c. problem to establish a set of initial conditions to produce real, physical results. The basic equations for d.c. analysis are well known equations; two current density equations for electrons and holes, two continuity equations for electrons and holes and Poisson's equation which are collectively referred to as the Van Roosbroeck model [9]:

$$J_e = qD_e\frac{dn}{dx} - q\mu_e\frac{d\psi}{dx} \qquad 1)$$

when used together

$$J_h = -D_h\frac{dp}{dx} - q\mu_h p\frac{d\psi}{dx} \qquad (2)$$

$$\frac{1}{q}\frac{dJ_e}{dx} + (G-U) = 0 \qquad (3)$$

$$\frac{1}{q}\frac{dJ_h}{dx} - (G-U) = 0 \qquad (4)$$

$$\frac{d^2\psi}{dx^2} = -\frac{q}{\varepsilon_o\varepsilon_r}(N_d - N_a + p - n) \qquad (5)$$

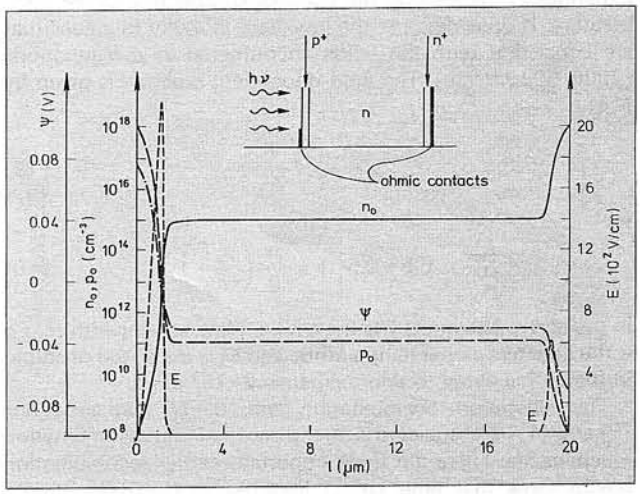

Fig. 1. Concentration profile, electrostatic potential and electric field across p^+-n-n^+ $Hg_{0.78}Cd_{0.22}Te$ photodiode at 77 K in the absence of infrared flux

In the above equations, J_e and J_h are the electron and hole current densities, μ_e and μ_h are the electron and hole mobilities, D_e and D_h are the electron and hole diffusion coefficients, n and p are the electron and hole carrier densities, ψ is the electrostatic potential, N_d is a concentration of donors and N_a is a concentration of acceptors, and $\varepsilon_o \varepsilon_r$ is the permittivity of the semiconductor. G and U denote the carrier generation and recombination rates, respectively. In calculations, nondegenerate Maxwell-Boltzmann statistics is assumed.

In order to execute a numerical analysis, expressions (1)–(5) were transformed into the form of differential equations in which the variables were defined as a finite number of division points. The mesh point spacing was defined as a function of the space coordinate x and changed from $1 \cdot 10^{-8}$ to $5 \cdot 10^{-8}$ m. Obviously, the quantities J_e, J_h, G and U in differential equations involve nonlinear functions of n, p and ψ. Such functions were linearized by Taylor's expression in variables n, p and ψ neglecting the higher order terms. It is known as Newton's iteration principle. More exactly, a description of this type calculation can be found in Kurata's monograph [8].

The mobility of carriers was computed by means of a two-step procedure [10] where a uniform low-field intrinsic mobility value is degraded by ionized impurity scattering and by high electric field behaviour. The ionized-impurity scattering limited mobility μ_{ii} is added into the low-field intrinsic mobility μ_{oi}

$$\frac{1}{\mu_o} = \frac{1}{\mu_{oi}} + \frac{1}{\mu_{ii}} \tag{6}$$

for both electrons and holes. Electron low-field intrinsic mobility can be approximated by [11]

$$\mu_{oe} = \frac{9 \cdot 10^8 b}{T^{2a}} \quad \text{with} \quad b = \left(\frac{0.2}{x}\right)^{7.5}; \quad a = \left(\frac{0.2}{x}\right)^{0.6} \tag{7}$$

where μ_{oe} is in cm²/Vs. For holes $\mu_{oh} = 400$ cm²/Vs is assumed.

The ionized-impurity scattering limited mobility can be determined by the Conwell-Weisskopf formulae [12, 13]

$$\mu_{ii} = \frac{64\pi^2 (\varepsilon_o \varepsilon_r)^2 (2kT)^{3/2}}{N_I Z^2 q^3 m_e^{*1/2}} \ln\left[1 + \left(\frac{12\pi\varepsilon_o \varepsilon_r kT}{Zq^2 N_I^{1/3}}\right)^2\right]^{-1} \tag{8}$$

where N_I is the total number of ionized centers per cm^{-3}, Z is the charge of the ions in units of q (i.e., +1, +2, etc), and m_e^* is the electron effective mass. For $T \geqslant 80$ K and $N_I \geqslant 10^{15}$ cm^{-3}, where the Conwell-Weisskopf and Brocks-Herring theories give comparable results, Eq. (8) is in reasonable agreement with other mobility theories [10], and such experimental data as are available [14].

The doping dependence of mobility is also corrected for field dependence by utilizing the concept of effective carrier temperature. It does degrade the low-field mobility to values that are consistent with the fields encountered in p-n junctions (2000–5000 V/cm). The field-dependent mobility is given by [15]

$$\mu = \mu_o \sqrt{\frac{T}{T_{ef}}} \tag{9}$$

where

$$\frac{T_{ef}}{T} = 0.5 + 0.5\left[1 + \frac{3\pi}{8}\left(\frac{\mu_o E}{C_s}\right)^2\right]^{1/2} \tag{10}$$

In the above equations T is the ambient lattice temperature, T_{ef} is the effective carrier temperature, and C_s is the speed of sound in the lattice equal to approximately $2 \cdot 10^5$ cm/s.

The generation-recombination term $(G-U)$ [see equations (3) and (4)] is associated with the predominant recombination mechanisms. There are three important carrier recombination mechanisms that limit carrier lifetimes in HgCdTe: Shockley-Read, radiative, and Auger recombination. In the Shockley-Read mechanism, recombination occurs via lattice defect and impurity energy levels within the forbidden energy gap of the semiconductor. These recombination sets can be controlled by the procedure used to grow the material; consequently, Shockley-Read recombination is not a fundamental limit to carrier lifetime.

The net recombination rate due to Shockley-Read states is given by [16]

$$(G-U)_{SR} = (pn - n_i^2)\left[\tau_{po}\left(n + n_i \exp\frac{E_t}{kT}\right) + \tau_{no}\left(p + n_i \exp\frac{-E_t}{kT}\right)\right]^{-1} \tag{11}$$

where τ_{no} and τ_{po} are the low-level minority carrier lifetimes due to SR processes and E_t is the trap-state energy level with respect to the intrinsic energy level. Throughout these calculations a midband-gap level was assumed. For p-type material $\tau_{po} \approx 100\ \tau_{no}$ and $\tau_{no} \approx 150$ ns can be assumed [16], for n-type material $\tau_{no} \approx \tau_{po} \approx 1$ μs is used [17, 18].

The radiative and Auger mechanisms are fundamental and are determined by the electronic band structure of the semiconductor. Humprey's papers [19, 20] indicate that due to reabsorption of photons, the effective radiative lifetime is largely extended, which means that the radiative generation-recombination is not important in narrow gap HgCdTe. Since the reabsorption conditions are specified for each real case and in general are not exactly known, in the present paper the $(G-U)$ term for radiative recombination is calculated in a traditional manner.

For the radiative recombination [21]

$$(G-U)_R = G_R (pn - n_i^2) \tag{12}$$

where

$$G_R = \frac{(2\pi)^{3/2}}{3} \frac{h\varepsilon_\infty^{1/2} q^2}{4\pi\varepsilon_o m^2 c^2} \left(\frac{m}{m_e^* + m_h^*}\right)^{3/2} \left(1 + \frac{m}{m_e^*} + \frac{m}{m_h^*}\right) \times \times \frac{E_g^2}{(kT)^{3/2} (mc)^{1/2}} \tag{13}$$

where m is the free electron mass and c is the speed of light.

The Auger recombination is classified in several processes according to related bands. The two most important mechanisms labelled Auger-1 and Auger-7 are dominant in n-type and p-type material, respectively. It can be shown that

$$(G-U)_A = (G_{A1} n + G_{A7} p)(pn - n_i^2) \tag{14}$$

where

$$G_{A1} = \frac{8(2\pi)^{5/2} q^4 m}{h^3 (4\pi\varepsilon_o)^2} \left(\frac{(m_e^*/m)|F_1 F_2|^2}{\varepsilon_r^2 (1+\mu)^{1/2} (1+2\mu)}\right) \frac{1}{n_i^2} \left(\frac{kT}{E_g}\right)^{3/2} \times \times \exp\left[-\left(\frac{1+2\mu}{1+\mu}\right)\frac{E_g}{kT}\right] \tag{15}$$

where $\mu = m_e^*/m_h^*$, G_{A1} and G_{A7} are the Auger coefficients for electrons and holes, respectively. $|F_1 F_2|$ is the overlap integral of periodic Bloch functions and is a term of great uncertainty-here the value of 0.2 has been assumed. Casselman and Petersen [22] have determined the ratio of Auger coefficients as

$$\frac{G_{A7}}{G_{A1}} \approx \frac{1 - 3E_g/2kT}{6(1 - 5E_g/4kT)} \tag{16}$$

which indicate that G_{A7} is several times lower when compared to G_{A1}.

A commonly used performance indicator for photovoltaic infrared detectors is the dynamic resistance at zero bias R_o given by

$$(R_o A)^{-1} = \left.\frac{dJ}{dV}\right|_{V_b = 0} \tag{17}$$

where A is the junction area. Because the basic parameters of photodiodes such as voltage responsivity and detectivity depend additionally on quantum efficiency η ($R_v \sim \eta R_o A$ and

$D^* \sim \eta (R_oA)^{1/2}$) [24], it is interesting therefore to analyze the effect of the structure of photodiode on quantum efficiency.

The magnitude of the quantum efficiency can be determined from relation [23]

$$\eta = \frac{J_{ph}}{q\Phi} \tag{18}$$

where Φ is the incident photon flux density connected with power density by relation $P = \Phi h\nu = (hc/\lambda)\,\Phi$.

The steady-state optical generation term is given by

$$G_{op} = (1-r)\,\eta\Phi \exp\left[-\int^{x} \alpha(y)\,dy\right] \tag{19}$$

where r is the reflectivity and $\alpha(y)$ is the position-dependent absorption coefficient. In our calculations we have assumed $r = 0$. The absorption coefficient must be evaluated separately for transitions involving heavy- and light-hole valence bands. We have used the expressions given by Anderson [24] which contain the Burstein-Moss factors.

The other material parameters of $Hg_{1-x}Cd_xTe$ which depend on the x-composition [such as $E_g(x,T)$, $n_i(x,T)$, $m_e^*(x,T)$, $m_{lh}^*(x,T)$] necessary in calculations have been determined according to Ref. [25].

3. Results and discussion

In this section, we will analyse the R_oA product and quantum efficiency for n^+-p-p^+ $Hg_{1-x}Cd_xTe$ photodiodes in dependence of the doping concentration and cutoff wavelength; consider the influence of different recombination mechanisms and tunneling on performance of photodiodes; and compare the results of our calculations with experimental data report by other authors. As a result of the utilization of high-quality HgCdTe material with good surface passivation, the experimental data presented here show diodes with high R_oA products.

The profiles of the electrostatic potential $\psi(x)$ and electric field $E(x)$ across p^+-n-n^+ $Hg_{0.78}Cd_{0.22}Te$ photodiode at 77 K ($\lambda = 10\ \mu$m), in the absence of bias voltage and IR flux, are shown in Fig. 1. As expected, the electric field is associated with the p^+-n junction. The characteristic of back-side field of the n-n^+ junction are also apparent in the profile.

The photonic behaviour of the photodiode can easily be examined by introducing an incident photon flux. This is done as shown in Fig. 2 for a non-biased p^+-n-n^+ $Hg_{0.78}Cd_{0.22}Te$ photodiode at 77 K using a front surface flux with power 0.1 W/cm^2 ($\Phi \approx 5 \cdot 10^{18}$ photons/cm^{2}s at $\lambda = 10.6\ \mu$m). We can see (Fig. 2a) that the concentration of majority carriers in the n-type region remains essentially unchanged, instead the concentration of minority carriers (holes) is nearly one thousand times greater. In addition, it should be noticed, that in the proximity of the p^+-n junction the minority carriers are extracted by the electric field of junction. This effect can be intensified when the photodiode has a reverse bias. Fig. 2b shows the net Auger, radiative, SR recombination rates and optical generation rate created by incident flux. The optical generation slowly decreases across the photodiode. Because of the higher doping level of the front surface (p^+) and back surface (n^+) regions, the Auger recombination mechanism is clearly dominant here and falls from a maximum value adjacent to the depletion edge of n-type base region, to essentially zero at the metal ohmic contacts. The other two recombination rate components also decay toward the contacts. In the depletion region of p^+-n junction, SR recombination is dominant. In the central n-type region with $N_d = 10^{15}$ cm^{-3}, Auger and radiative recombinations have comparable rates. In the case of higher donor concentrations, the Auger recombination will be decisive.

The dependence of the R_oA product components and quantum efficiency on the dopant concentrations in central n-type base region for p^+-n-n^+ $Hg_{0.78}Cd_{0.22}Te$ photodiode at 77 K are shown in Fig.3. The $(R_oA)_T$ component has been calculated assuming Anderson theory [26] for direct interband tunneling for asymmetrical abrupt p-n junctions in the InSb-like semiconductors. The trap-assisted tunneling is not analyzed because donor activation energies are generally not observed in n-type HgCdTe material. The main contribution in determination $(R_oA)_{ef}$ had Auger process. The influence of Auger process is unexpectedly high, which is conditioned by frontal p^+-type region.

To obtain the possibly higher value of the R_oA product, a technological process of photodiode preparation should be performed to obtain donor concentrations in the base region below 10^{16} cm^{-3}. However, at donor concentrations just below 10^{16} cm^{-3}, the quantum efficiency is low due to strong band filling. The influence of the Burnstein-Moss effect on quantum efficiency is more exactly shown in Fig. 4. To obtain quantum efficiency near the absorbtion edge, a donor concentration of about 10^{15} cm^{-3} is required.

Taking the above into consideration the optimum doping concentration for the n-type base region of p^+-n-n^+ LWIR photodiodes operated at 77 K is about 10^{15} cm^{-3}. This concentration can also be assumed as optimal for photodiodes at lower temperatures with cutoff wavelength between 7 and 15 μm.

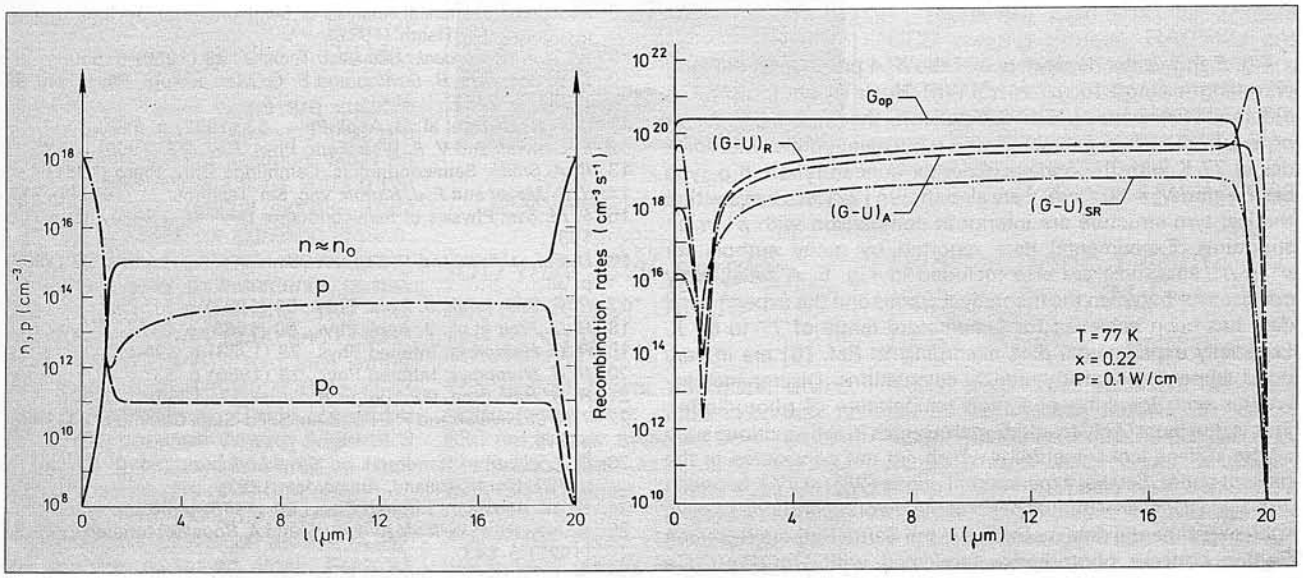

Fig. 2. p^+-n-p^+ $Hg_{0.78}Cd_{0.22}Te$ non-biased photodiode characteristics at 77 K in the presence of incident flux $5 \cdot 10^{18}$ photons/cm^2 s: a) electron and hole concentration vs position; b) net recombination rates and optical generation vs position

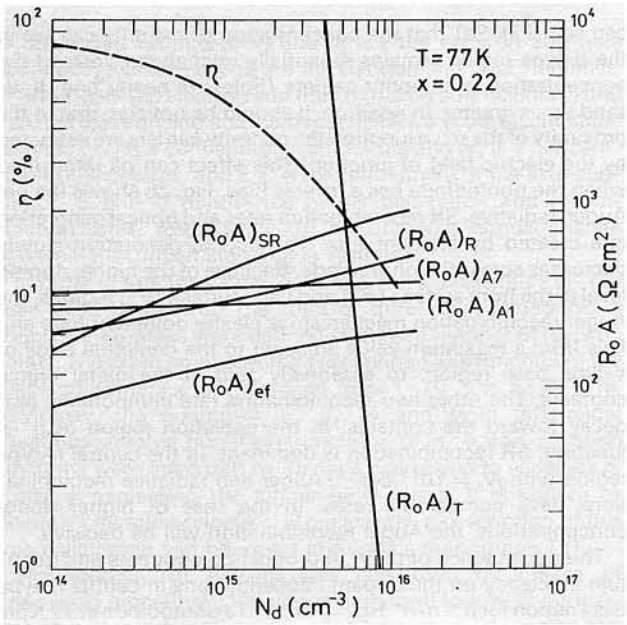

Fig. 3. The dependence of the R_oA product and quantum efficiency η on donor concentration in central n-type base region of p^+-n-n^+ $Hg_{0.78}Cd_{0.22}Te$ photodiode ($\lambda_c = 10.6\ \mu m$) at 77 K

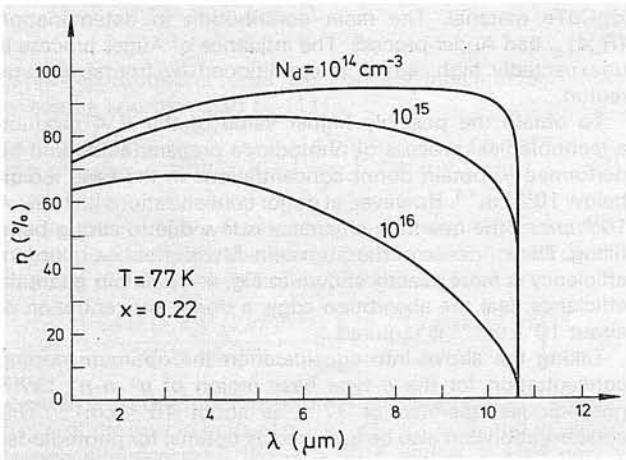

Fig. 4. The dependence of quantum efficiency η on donor concentration in central n-type base region of p^+-n-n^+ $Hg_{0.78}Cd_{0.22}Te$ photodiode at 77 K

Fig. 5 shows the dependence of the R_oA product on the long wavelength cutoff for p^+-n-n^+LWIR HgCdTe photodiodes at different temperatures. For comparison, theoretical curves for n^+-p-p^+ (the same geometry) and n^+-p semiinfinite photodiodes at 77 K with the optimal acceptor concentration in p-type base region $N_a = 10^{16}$ cm^{-3} are also shown [27]. We can see that the last two structure are inferior in comparison with p^+-n-n^+ structures. Experimental data reported by many authors for p^+-n-n^+ structures are also included in Fig. 5. A satisfactory consistence between the theoretical curves and the experimental data has been achieved for temperature range of 77 to 60 K. Especially experimental data according to Ref. [6] are in very good agreement with theoretical calculations. Discrepancy increases with lowering operation temperature of photodiodes. This is due most likely to additional currents in the junctions such as the surface leakage current which are not considered in the present paper. Several experimental points [28], at 77 K between $7 < \lambda < 10\ \mu m$, are situated beyond the theoretical curve. Largely such experimental data measured at the Santa Barbara Research Center, concern photodiodes fabricated with HgCdTe/CdTe heterostructures. In this case the gradient of composition in the proximity of CdTe substrate can improve blocking properties of n-n^+ backside junction, which results in increase R_oA product.

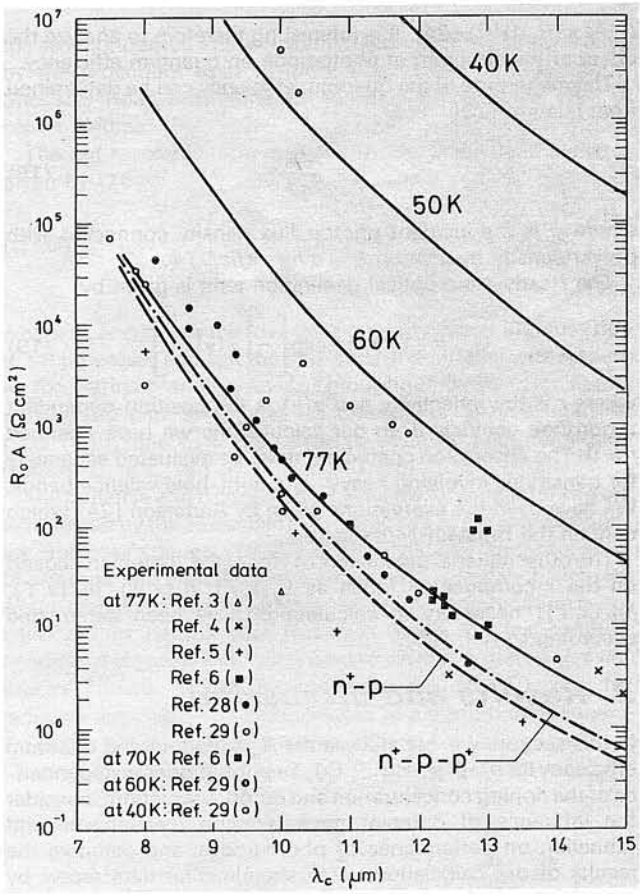

Fig. 5. The dependence of the R_oA product on the long wavelength cutoff for LWIR p^+-n-n^+ HgCdTe photodiodes. The experimental data are taken from Refs [3–6, 28 and 29]. For comparison $R_oA = f(\lambda_c)$ for n^+-p and n^+-p-p^+ junctions (with $N_a = 10^{16}$ cm^{-3}) are shown

References

1. *A. Rogalski* and *W. Larkowski*: Electron Technology, **18** (1985) p. 55.
2. *A. Rogalski* and *J. Piotrowski*: Prog. Quantum Electron., **12** (1988) p. 87.
3. *J. M. Arias* et al.: J. Appl. Phys., **65** (1989) p. 1747.
4. *L. O. Bubulac* et al.: Semicon. Sci. Technol., **5** (1990) p. S45.
5. *J. Arias* et al.: J. Appl. Phys., **69** (1991) p. 2143.
6. *G. N. Pultz* et al.: J. Vac. Sci. Technol., **B9** (1991) p. 1724.
7. *C. C. Wang*: ibid. [6] p. 1740
8. *M. Kurata*: Numerical Analysis of Semiconductor Devices. Lexington Books, DC Heath (1982).
9. *W. Van Roosbroeck*: Bell Syst. Tech. J., **29** (1950) p. 560.
10. *C. J. Summers, B. Darling* and *B. G. Martin*: Appl. Phys. Lett., **59** (1986) p. 2457.
11. *J. P. Rosbeck* et al.: J. Appl. Phys., **53** (1982) p. 6430.
12. *E. Conwell* and *V. F. Weisskopf*: Phys. Rev., **77** (1950) p. 388.
13. *R. A. Smith*: Semiconductors. Cambridge Univ. Press (1961).
14. *J. R. Meyer* and *F. J. Bartoli*: Vac. Sci. Technol., **21** (1982) p. 237.
15. *S. M. Sze*: Physics of Semiconductor Devices. J. Wiley, New York 1981.
16. *D. E. Lacklison* and *P. Capper*: Semicond. Sci. Technol., **2** (1987) p. 33.
17. *R. G. Pratt* et al.: J. Appl. Phys., **54** (1983) p. 5152.
18. *R. G. Pratt* et al.: J. Appl. Phys., **60** (1986) p. 2377.
19. *R. G. Humpreys*: Infrared Phys., **23** (1983) p. 171.
20. *R. G. Humpreys*: Infrared Phys., **26** (1986) p. 337.
21. *R. N. Hall*: Proc. IEE 106, pt B, Suppl. **17** (1960) p. 923.
22. *T. N. Casselman* and P. E Petersen: Solid-State Commun., **33** (1980) p. 615.
23. *C. T. Elliott*: in Handbook on Semiconductors (ed. C. Hilsum), **4**, p. 727, North-Holland, Amsterdam 1982.
24. *W. W. Anderson*: Infrared Phys., **20** (1980) p. 363.
25. *A. Jóźwikowska, K. Jóźwikowski* and *A. Rogalski*: Infrared Phys., **31** (1991) p. 543.
26. *W. W. Anderson*: Infrared Phys., **20** (1980) p. 353.
27. *A. Rogalski*: Infrared Phys., **28** (1988) p. 139.
28. *P. R. Norton*: Opt. Eng., **30** (1991) p. 1649.
29. *C. C. Wang*: Fermionics Corporation (unpublished).